Austin Publishing Group

Review Article

Retinal Identification using Shearlets Feature Extraction

Modarresi M¹*, Oveisi IS² and Janbozorgi M³
¹Department of Biomedical Engineering, Medical Sciences University, Tehran
²Department of Biomedical Engineering, Science and Research, Islamic Azad University, Tehran
³Department of Medical Sciences, Washington State University, USA

*Corresponding author: Modarresi M, Department of Biomedical Engineering, Medical Sciences University, Tehran

Abstract

Since the fundamental features of retinal images are comprised of different orders and locations, in this paper, we attempt to analyze retinal images by means of a multi-scale method, which is based on shearlets transform that is an effective directional multi-scale system for image assessment. This method was demonstrated improvement in image discontinuities, for example, edges and corners at numerous scales. Movement effects of the eyeball occurring during the scanning process encouraged us to employ a method based on the Radial Tchebichef Moments so as to estimate and eliminate the effects rotation angle of the head or eyeball movement may introduce in the scanning process. After this, localizing the optic disc and eliciting the Region of Interest (ROI) intended to acquire similar parts within different retinal images from the same person, a rotation invariant template can be achieved from each ROI retinal sample. The *Mahalanobis* distance is utilized in the proposed method to assess the biometric pattern similarity. The experimental results shower = 0.0024 in retinal identification. These results are a testimony of the power and efficacy of the proposed approach.

Keywords: Biometric; Retinal identification; Shearlets transform; Radial tchebichef moments; *Mahalanobis* distance
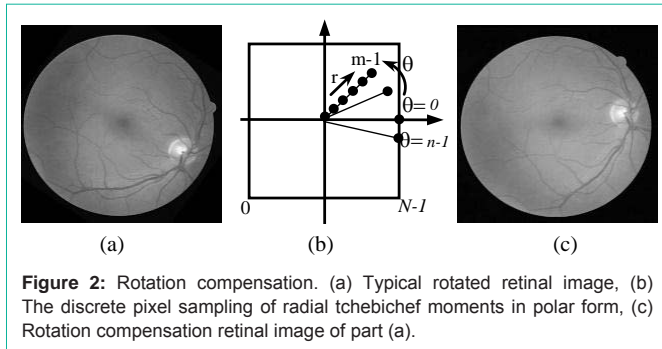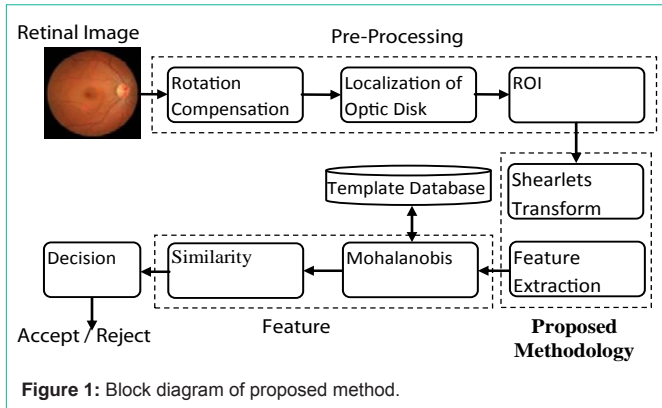
Introduction

Dependable verification of individuals has transformed into a fundamentally valuable service in a scope of regions, in police or military settings as well as in non-military personnel (civilian) applications, for example, money related exchanges methodology or access control too. Traditional authentication systems rely on either knowledge, such as a password or a PIN number or possession such as a card or a key. However, such systems are far from reliable for a number of environments as they are inherently incapable of distinguishing between a true-authorized user and an intruder who have fraudulently obtained the privilege of the authorized user. A solution to these deficiencies has been found to lie in the biometric-based authentication technologies. The match between a biometric and a specific application depends on the operational mode of the application and the properties the biometric characteristic possesses. Biometrics popularly used includes face and speech recognition, fingerprint, iris. Among these biometrics, the retina surpasses others, allowing for higher-precision recognition, which is owing to its uniqueness and the fact that the blood vessel pattern remains unchanged during one's life [1]. Conventional strategies for multiscale signal dissection and time-frequency representation, wavelets and Gabor transforms have been broadly utilized as a part of image processing requisitions. Nonetheless, these techniques are not prepared to do productively catching directional characteristics from data because of their restricted directional affectability. On the contrary, shearlets transform, as our method, can examine images characterized at different orientations as well as toward different scales; they give acceptable effective mathematical techniques with location singularities for example, image edges.

This paper is organized as follows: Section II gives a synopsis of related works. Section III presents system architecture. In Section IV, the preprocessing of retina image is expounded. Section V and Section VI are devoted to proposed methodology and feature matching, respectively. Experimental results are presented in Section VII. Finally, Section VIII includes conclusion and future work.

Related Work

The advantage of using retina over other biometric traits is its broad application in both recognition/authentication systems and the medical field. Several methods have been suggested for retina recognition. Because of limitation, we only refer to some of them. The Matched Filter approach [2] where an intensity profile, approximated by a Gaussian filter, is associated with the gray-level profiles of the cross-sections of retinal vessels. Yet, blood vessels suffer from poor local contrast and hence applying the edge detection algorithm does not produce satisfactory results in retinal recognition system. Ridge based vessel segmentation method [3] works based upon extraction of image ridges, which coincide, with a degree of approximation, with vessel centerlines, there are still similar limitations. Oinonen *et al.* [4] proposed a method based on minute features. The method included three steps: Blood vessel segmentation, feature extraction and matching. In fact, vessel segmentation serves as a preprocessing to feature extraction. Further, vessel crossings along with their orientation information were obtained. This information was coordinated with the relating ones from the examination image. The computational time of this method is considered to be high; also this method was used in verification mode. Widjaja [5] proposed another technique for noise ruined lower contrast retinal pictures recognition by utilizing the "Compression-Based Joint Transform Correlator" (CBJTC). The noise strength is accomplished by correlating wavelet transform and retinal object and source images which have low spatial frequencies are improved by utilizing the dilated wavelet filters. In work directed by waheed *et al.* [6], two diverse methodologies for

Figure 1: Block diagram of proposed method.

Figure 2: Rotation compensation. (a) Typical rotated retinal image, (b) The discrete pixel sampling of radial tchebichef moments in polar form, (c) Rotation compensation retinal image of part (a).

Figure 3: Localization of optic disc based on template matching. (a) A typical retinal image (b) Close up view of the template image (c) Correlated image (d) Correlation coefficients values.

retinal recognition were utilized. First place technique, is a vascular-based feature extraction which utilizes minutiae points with an enhanced vessel extraction utilizing *2D*-Gabor wavelets. While, non-vascular based strategy means to dissect non-vessel properties of retinal pictures with a specific end goal to decrease time perplexity which removes novel basic features from retinal color pictures by utilizing the basic data of retinal pictures same as luminance, contrast, and structure.

System Architecture

Figure 1 shows different parts of our intended biometric retinal identification. In this paper, in order to bolster the actual performances for biometric identification systems, we proposed rotation compensation method based on Radial Tchebichef Moments and by localization of optic disc, it is possible to identify the retinal region of interest to make the rotation-invariant template from each retinal sample. The proposed method makes use of *Mahalanobis* distance to evaluate the biometric pattern similarity; afterwards, the person's identification is achieved through matching score maximization. Owing to its properties providing marked advantages for biometric data, in particular, the rotation compensation as well as feature correlation exploiting, special *Mahalanobis* distance makes a suitable alternative for the biometric pattern matching.

Pre-Processing

Rotation compensation

The major problem associated with using retinal images for identification arises from the inherent possibility of the eye moving in front of the fund us camera, resulting in having two different images coming from one person. This deficiency can be surmounted
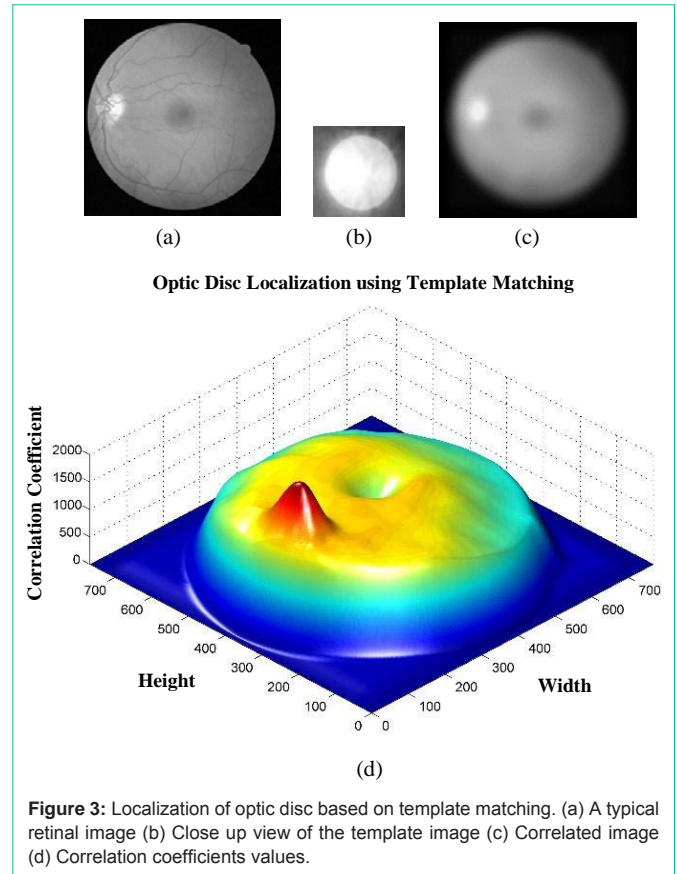
using a method based on the Radial Tchebichef Moments [7] in our work, which allows estimating the rotation angle compensation of either head or eye movement. This plan utilizes the region and the greatest radial distance of a pattern to normalize the Radial Tchebichef Moments. (Figure 2a) portrays the typical rotated retinal image, (Figure 2b) depicts the discrete pixel sampling of Radial Tchebichef Moments in polar form and (Figure 2c) illustrates the rotation compensation associated with the right eye retinal image. Customarily m has an amount, which is at minimum *N/2*, and *n* is at 360 when the picture is sampled at single degree intervals.

Localization of optic disc

Template Matching is a popular technique, which is used to isolate certain features in an image. The execution includes a correlation of primary image and an appropriately picked template [8]. The most apt match is then localized based upon some criterion of optimality. Regarding the size of the optical plate local in our retinal dataset images, we made a 68 × 68 pixels template picture by taking an average over the optic plate local in 25 retinal images, each chose from our image dataset (Figure 3b). This was performed by using of grey levels exclusively owing to the fact that the result is computationally less expensive and possesses sufficient accuracy. The normalized Correlation Coefficient (CC) has the following definition:

$$R(i,j) = \frac{\sum_k \sum_l \left(f_{k+i,l+j} - \overline{f_{i,j}} \right)\left(t_{k,l} - \bar{t} \right)}{\left\{ \left(\sum_k \sum_l \left(f_{k+i,l+j} - \overline{f_{i,j}} \right)^2 \right)\left(\sum_k \sum_l t_{k,l} - \bar{t} \right)^2 \right\}^{0.5}} \quad (1)$$

where *f* and *t* denote the original image and the template respectively,
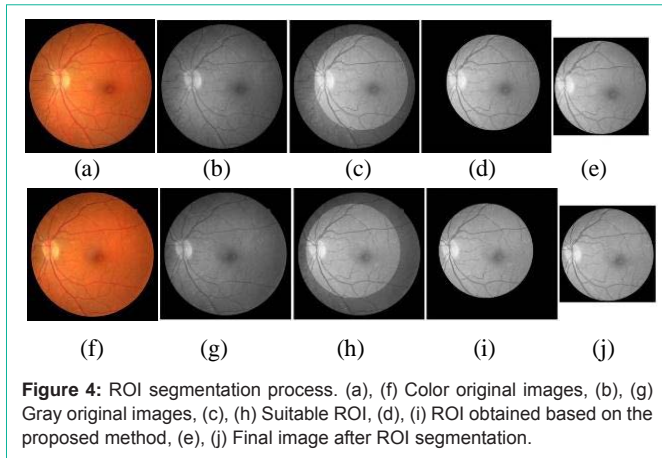
Figure 4: ROI segmentation process. (a), (f) Color original images, (b), (g) Gray original images, (c), (h) Suitable ROI, (d), (i) ROI obtained based on the proposed method, (e), (j) Final image after ROI segmentation.

$\overline{t}$ represents the template pixels mean value; likewise $\overline{f}$ represents the image pixels mean value in the region, and is defined by the template location [8]. Here, for every retinal image we quantified the normalized correlation coefficients to give a sign of how much the template picture and every individual pixel in the picture under study are coordinated. (Figures 3a & 3c) demonstrate a typical retinal image along with its evaluated normalized CC values. As can be seen, the optic disc region is highlighted for distinction. The highest matched point is displayed as the brightest point in the correlation image (Figure 3d). We assume this point's coordinates as a viable candidate for the location of the optic disc center. The highest reference point is required to obtain ROI segmentation so that explanation in the next section.

Region of Interest (ROI) Segmentation

All The involuntary eyeball movements in the scanning process can potentially produce different images taken from the same individual, which means that some parts of the first image may not be present in the second image and vice versa. To obviate this disadvantage and eliminate the background from images, we are to find Region of Interest (ROI).

In (Figure 4) two different retinal-image samples from the same person in our database are illustrated, and the ROI segmentation process in two various images of the left eye of the same person. Here, ROI segmentation is achieving as following steps:

Step-1: Color retinal fund us image is converting into a gray image from the green channel.

Step-2: Compensate the rotation of retinal image.

Step-3: Find the optic disc with template matching algorithm.

Step-4: Compute the CC in the optic disc.

Step-5: At a distance of 50 pixels from the highest reference point (CC) in optic disc, a circle area (search space) with 500 pixels diameter in order to extract ROI was drawn. The final size of each image is 512×512. The ROI area consists of common points in both different images of the same person (Figures 4e & 4j).

Proposed Methodology

Shearlets transform

Signal assessments in both time and frequency domains, wavelet and Gabor transforms; have gotten critical consideration in the most recent decades. Though, a detriment of these strategies is their restricted directional affectability - their constrained ability of assessing to directional components. A few varieties of wavelets transform have been proposed to beat these confinements, like directional wavelets, bandelets, brushlets, contourlets, phaselets, directionlets, ridgelets and curvelets. Shearlets [9] have imperative properties, for example, they are ideal clinched alongside approximating *2D* smooth function works with discontinuities along C^2 - curves Furthermore they structure a relative framework. Shearlets transform gives a general structure to assess information with anisotropic data at different scales. As a result, flag singularities, for example, edges, could be distinguished and situated in images. In dimension=2, the continuous shearlets transform of an (Figure 1) is characterized likewise the mapping [9]:

$$SH_\phi I(a,s,t) = <I, \phi_{a,s,t}>, \ a>0, \ s \ \epsilon \ R, \ t \ \epsilon R^2, \quad (2)$$

where the evaluating factor $\phi_{(a,s,t)}$ will be known as shearlet basis, which is delineated as:

$$\phi_{a,s,t}(x) = \left|\det M_{a,s}\right|^{\frac{-1}{2}} \phi\left(M_{a,s}^{-1} x - t\right), \quad (3)$$

where:

$$M_{a,s} = (B_s A_a) = \begin{pmatrix} a & s\sqrt{a} \\ 0 & \sqrt{a} \end{pmatrix}; \ A_a = \begin{pmatrix} a & 0 \\ 0 & \sqrt{a} \end{pmatrix}, \ B_s = \begin{pmatrix} 1 & s \\ 0 & 1 \end{pmatrix}.A_a$$

A_a is called as the anisotropic dilation matrix and B_s will be the shear matrix. Every component $\phi_{(a,s,t)}$ has a frequency bolster (support) on a couple of trapezoids at a lot scales, symmetric regarding the source (locations), and oriented along a line of slope *s*. Consequently, the shearlets $\phi_{(a,s,t)}$ shape a gathering of well-localized waveforms at different scales *a*, orientations *s* and locations *t*. As follows, shearlets can distinguish directional data and account for the geometry of multidimensional functions, which solved those constraints of the wavelets transform [9].

Feature extraction

Because of the iterated low pass filtering, the Grey-Level Co-Occurrence Matrices (GLCM) texture data with higher congruity has been isolated; subsequently the texture data are mainly contained in the directional sub-bands of every scale. Thusly, the low pass picture is disregarded while ascertaining the texture component vector. A set of statistical texture features introduced in literature are used in this study as an assessment criterion. These features set are including: Correlation (*Co*), Uniformity (*Un*), Entropy (*Ent*), Dissimilarity (*Dis*) and Cluster Shade (*Sh*) which are used for the shearlets space express as follow [10].

$$CO = \sum_{i=1}^{N-1}\sum_{j=1}^{N-1} \frac{(i-\mu_x)(j-\mu_y)C_{ij}}{\sigma_x \sigma_y} \quad (4)$$

$$Un = \sum_{i=1}^{N-1}\sum_{j=1}^{N-1} C_{ij}^2 \quad (5)$$

$$Ent = -\sum_{i=1}^{N-1}\sum_{j=1}^{N-1} C_{ij}\left|i-j\right| \quad (6)$$

$$Dis = \sum_{i=1}^{N-1}\sum_{j=1}^{N-1} C_{ij}\log C_{ij} \quad (7)$$

$$Sh = \sum_{i=1}^{N-1}\sum_{j=1}^{N-1}\left\{i+j-\mu_x-\mu_y\right\}^3 \times C_{ij} \quad (8)$$

where C_{ij} indicates co-occurring probabilities stored inside GLCM. Also, (μ_x, μ_y) and (σ_x, σ_y) represent means and standard deviations for row I and column j within GLCM. Consequently, the final feature vector of the sub-band image (R_{mk}) on the kth sub band at the mth shearlets level of decomposition is defined as:

$$R_{mk} = \left\{ A_{mk}, B_{mk}, C_{mk}, D_{mk}, E_{mk} \right\} \quad (9)$$

Feature Matching

Distance matching scores

Feature Matching involves comparing the Feature vector, which is generated for the query image, provided in the testing phase, versus stored feature vector in the database that is obtained during the training phase. The matching phase of the retinal identification process necessitates the following steps [11]:

1. Computing the distance $d(x,z)$ extending between the retinal template z and the real test retinal sample x;

2. Performing distance score normalization.

3. Converting distance to similarity-score.

4. Computing the set of similarity scores for identification (1: N).

So as to calculate the distance score between the biometric template z and the current biometric test x, *Mahalanobis* distance was utilized, which is given by [12]:

$$d_M\left(x,z\right) = \sqrt{\left(x-z\right)^T.\left(\sum\left(x-z\right)\right)^{-1}} \quad (10)$$

where Σ is two retinal feature vectors covariance matrix:

$$\sum = \text{cov}\left(x,z\right) = E[\left(x - E\left[z\right]\right).\left(x - E\left[z\right]\right)]^T \quad (11)$$

The reason we chose to use this distance metric in the feature vector space was owing to its principal properties, scaling invariance and feature correlation exploiting [12]. The first property is paramount specifically because the application needs to scale the features so that it can compare them against different individuals and to investigate the features contribution on the identification accuracy. The second property gains significance as it allows an earlier selecting for the optimal feature subsets, which is based on their correlation.

Feature extraction

The distance score normalization serves to provide a common value range of all matching scores which will be computed for the biometric patterns. There are numerous normalization techniques available, such as *Z*-Score, decimal scaling, Min-Max, sigmoid normalization, etc. For our available biometric data, we opted for the double sigmoid function, given by:

$$D\left(x,z\right) = \begin{cases} for d_M\left(x,z\right) < \theta : \dfrac{1}{1 + A_1.\exp\left[-B_1.\left(\dfrac{d_M\left(x,z\right) - \theta}{C_1}\right)\right]} \\ for d_M\left(x,z\right) \geq \theta : \dfrac{1}{1 + A_2.\exp\left[-B_2.\left(\dfrac{d_M\left(x,z\right) - \theta}{C_2}\right)\right]} \end{cases} \quad (12)$$

where

1. The coefficients A_1, A_2, B_1 and B_2 are attained from the experimental data; they are in fact shape parameters for the sigmoid function.

2. C_1 and C_2 represent the quasi-linear behavior region boundaries for the sigmoid function, these parameters are obtained from the experiment as well.

3. Θ is a threshold value related to the security level, which is set for the application.

The normalized distance score is acquired by measuring the difference between the test retinal feature vector x and the compared biometric template z.

Distance to similarity conversion

In order to determine the similarity or the level of matching between the current biometric sample x and the biometric template z, it is essential to apply an additional transform so that the highest scores would mean more similarity while the lowest scores would translate as larger difference. All the computed scores vary in the range [0,1], as governed by the property of the sigmoid function. Owing to this range, the distance-to-similarity conversion can be performed by:

$$S = s(x,z) = 1 - D(x,z) \quad (13)$$

Set of the similarity scores

We are computing N scores for each person to be identified, the comparison being *1:N*. Thus, the identification similarity scores are given by:

$$S_i = \begin{cases} for d_{M,i}\left(x,z_i\right) < \theta : \dfrac{A_1.\exp\left[-B_1.\left(\dfrac{d_{M,i}\left(x,z_i\right) - \theta}{C_1}\right)\right]}{1 + A_1.\exp\left[-B_1.\left(\dfrac{d_{M,i}\left(x,z_i\right) - \theta}{C_1}\right)\right]} \\ for d_{M,i}\left(x,z_i\right) \geq \theta : \dfrac{A_2.\exp\left[-B_2.\left(\dfrac{d_{M,i}\left(x,z_i\right) - \theta}{C_2}\right)\right]}{1 + A_2.\exp\left[-B_2.\left(\dfrac{d_{M,i}\left(x,z_i\right) - \theta}{C_2}\right)\right]} \end{cases}, i = \overline{1, N} \quad (14)$$

Experimental Results and Analysis

The experimental database

In this work, all our experiments were implemented in MATLAB with 4.2GHz CPU, and 8GB memory. Experiments utilized a self-built database containing 5000 retinal images taken from 500 different people (10 images with different rotations ranges). In order to test and analyze our proposed algorithm under real conditions, we used the digital fund us camera that existed in our country with *TopCop* brand, in over a time span of three years. Therefore, our self-built database permissions the frame work to be tried in entirely hard conditions and recreating a more sensible and practical environment. These retinal images were taken from people of different ages and both genders and encompass all the potential diseases which may have any tangible effect on the retinal. The diverse conditions are additionally considering the way that distinctive specialists with various contrast and illumination designs on the camera have gained the pictures. Six of these were utilized to train the template and the staying four samples were utilized for testing.

In order to evaluate the robustness in terms of rotation invariance, we rotated our database. The three rotation angles used are $\pm$ 15º, $\pm$ 25º, $\pm$ 35º. The size of the original retinal images was 700×700
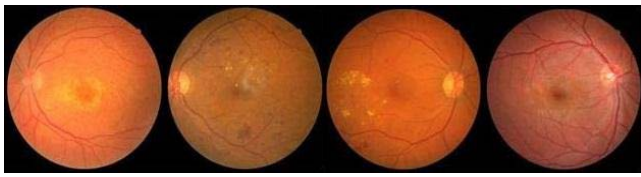
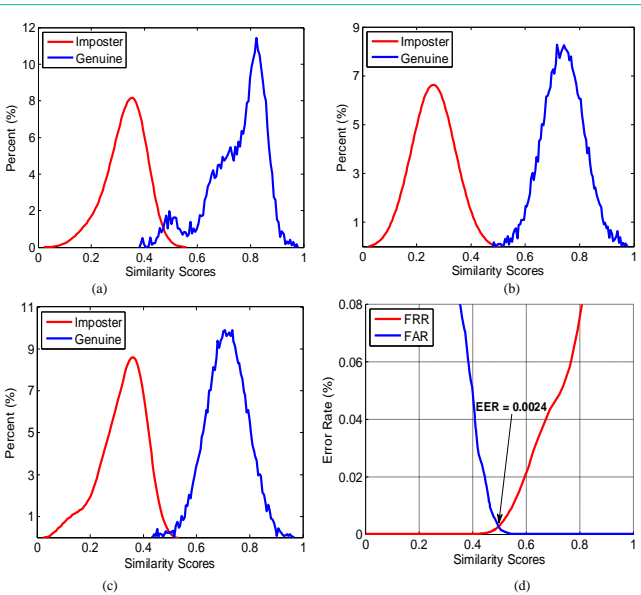**Figure 5:** Some different individual's samples of our database.

Figure 6: Genuine and imposter distribution of the *2nd* to *4th* shear lets decomposition level. (a) *2nd* level (b) *3rd* level (c) *4th* level (d) FAR vs. FRR curve for proposed method.

Figure 7: Receiver Operating Characteristics (ROC), while 2, 3, 4, 5 and 6 training images are utilized to train of the proposed method in *3rd* level of shearlets decomposition.

Table 1: Time cost for every step and overall-time of identification for every individual.

Steps	Time (sec)
Image Capturing	0.2
Rotation Compensation	0.3
Localization of Optic Disc	0.2
ROI Segmentation	0.7
Feature Extraction	1.2
Feature Normalization	0.8
Feature Matching	1.3
Overall Identification Time	**4.7**

Table 2: Decidability record and genuine and imposter statistical measures.

Training images	μ_G	μ_I	σ_G	σ_I	d'	EER
2	0.241	0.942	0.172	0.125	4.656	0.1594
3	0.199	0.918	0.167	0.120	4.939	0.1238
4	0.164	0.911	0.145	0.117	5.642	0.0721
5	0.147	0.908	0.123	0.122	6.196	**0.0024**
6	0.140	0.901	0.114	0.125	6.356	0.0322

pixels. Referring to the brightest pixels, the ROI mask is calculated. Therefore, the final retinal images are resized to 512×512 pixels. Figure 5 shows some different individual's samples of the right and left eyes from our database.

Retinal identification

The genuine and imposter matching's were employed to evaluate the most desirable level of shearlets decomposition. Within this mode, the input retina's class is recognized, with each sample being matched against all the other samples from the same subject as well as all samples coming from the other 500 subjects. Provided the two matching samples originate from the same subject, the successful matching is called a genuine or intra-class matching. Otherwise, interclass matching or imposter is the term designated to the unsuccessful matching. Accordingly, we make use of full matching in intra class, where each sample is matched with all the other samples within the same class, and interclass matching, where each of the samples is matched against all the samples from the other 500 subjects. An aggregate of 1,000,000 (500×500×4) matching were performed, 2000 (500×4) of which accounted for genuine matching. The genuine and imposter deliveries corresponding to the 2nd, 3rd and 4th level of shearlets decomposition are setup in (Figures 6a-6c) respectively. As is apparent and can be seen the 3rd level of shearlets decomposition is devoid of the over lapped area, hence, this level is expected to demonstrate the highest performance in our identification system. Additionally, in our paper, the False Accept
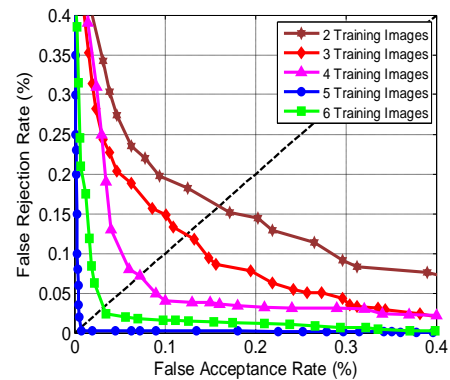
Rate (FAR) versus False Reject Rate (FRR) is shown in (Figure 6d). In 1 to 500 matching, all of the 2000 (500×4) testing images were used, and EER=0.0024 in 3rd level of shearlets decomposition was obtained. This figure is a testimony of the approach excellent performance in retinal identification.

Furthermore, (Table 1) records every step-time and over all-time cost of identification for each person in the proposed algorithm.

Evaluating the number of training images

The genuine and imposter disseminations are appearing in (Figure 7) while 2 to 6 training images are utilized to train of the proposed method in 3rd level of shearlets decomposition, respectively. This figure de-lineate their Receiver Operating Curve (ROC), which demonstrates the variety of the FAR vs FRR at various working thresholds. Moreover, the EER is utilized to quantify the framework performance that is characterized as the error rate when the FAR and the FRR are equivalent. In next section, (Table 2), demonstrates the consequences of EER from every utilizing number of training images.
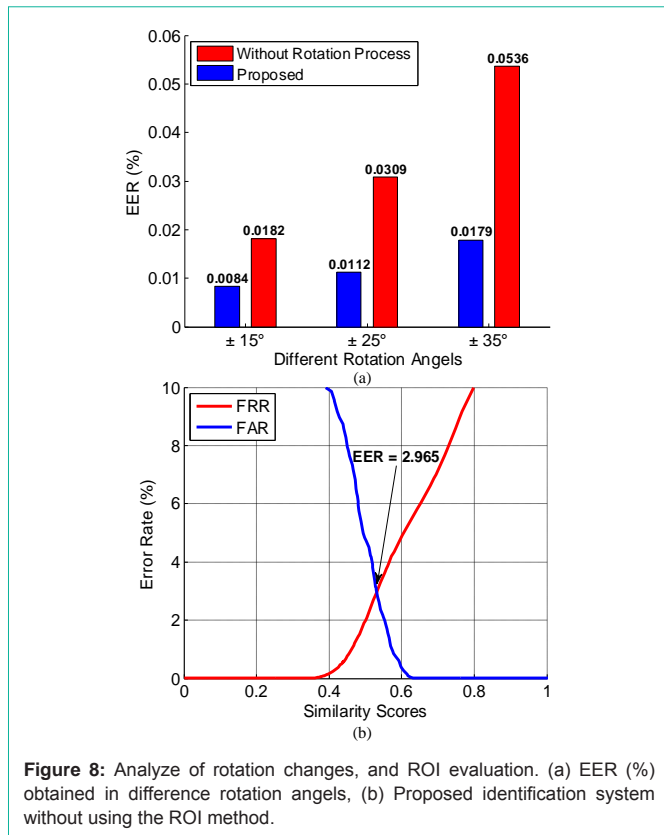
Figure 8: Analyze of rotation changes, and ROI evaluation. (a) EER (%) obtained in difference rotation angels, (b) Proposed identification system without using the ROI method.

From these outcomes, it can be inferred that the system can work productively even with just two training images at EER of 0.1594%. It can likewise be watched that utilizing five training images can give better accuracy in identification mode. This can be clarified by the way that, the utilization of more than two retinal pictures brings about more information being caught in every class. Nonetheless, utilizing more than five training images does not give further betterment (Table 1).

Separability test

Decidability Index provides an excellent measure for the separability of Genuine and Imposter classes. Assuming μ_G and μ_I respectively denote the mean value of Genuine and Imposter Distributions, and also σ_G and σ_I represent the standard deviations of genuine and imposter, respectively, we will then have the decidability d¹ defined as [13]:

$$d' = \frac{|\mu_G - \mu_I|}{\sqrt{\dfrac{\sigma_G^2 - \sigma_I^2}{2}}} \qquad (15)$$

The greater the decidability record the more prominent being kept apart of genuine and imposter appropriations. The decidability indicator and all of statistical measures (i.e., means and standard deviations) in different number of training images are abridged in (Table 2). The outcomes show that utilizing five and six training images in 3rd level of shearlets decomposition deliver the best division, respectively.

The rotation and ROI analysis

In order to the observed the robustness of rotation changes of

Table 3: Results of different identification methods.

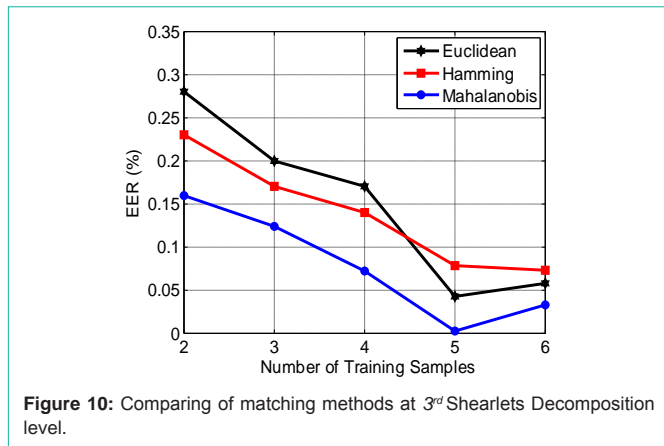| Method	Number of Subjects	Running time (sec)	Accuracy (%)
Waheed [6]	20	-	99.57
Sukumaran [14]	40	3.1	98.33
Meng [15]	59	7.81	EER = 0
Köse [16]	80	-	95
Xu et al. [17]	-	277.8	98.5
Proposed Method	**500**	**4.7**	**EER = 0.0024**
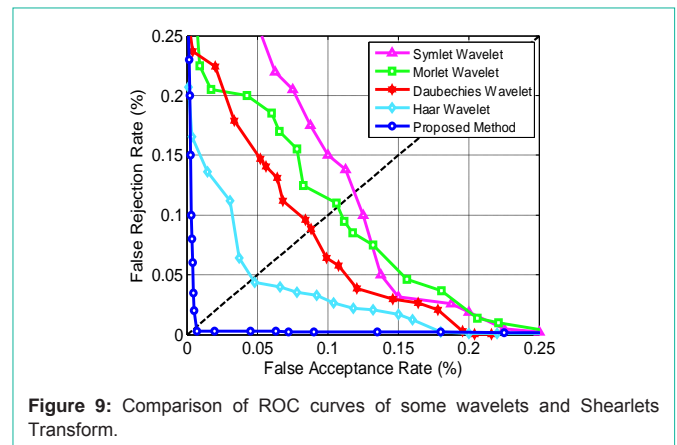
Figure 9: Comparison of ROC curves of some wavelets and Shearlets Transform.

the proposed algorithm, we lead the other check on our data set. From (Figure 8a) it can be observed that, for the proposed technique in 3rd level of shearlets decomposition, however the estimations of EER fluctuates as per rotation changes, but these plots demonstrate that the proposed design structure is vigorous to rotation changes. It should be noted that, rotation experiment done while we have used the ROI section (Table 2).

The sharp differences between the values of the blue and red bars show the importance and impact of using proposed methods. Additionally, in order to highlight the significance of the ROI method in the proposed identification system, assessment was directed by using ROI method and without using ROI method, they got aftereffects of which are graphically shown in (Figure 6d) and (Figure 8b), respectively, so that (Figure 6d) illustrates the FAR vs FRR curve when the ROI method is existent and (Figure 8b) depicts the FAR vs FRR curve when the system is non-existent of the ROI method. Also, both (Figures 6d & 8b) experiments done while we have used the rotation section. Consequently, the EER value of rotation and ROI method show the significance of these sections in our proposed method (Table 3).

Transforms performance comparison

In this section, we assess the execution of our proposed algorithm taking into account shearlets transform, and contrasting it with Haar wavelet, Daubechies wavelet, Morlet wavelet, and Symlet wavelet. For a number of tests run, the typical ROC curves of the experimental results are illustrated in (Figure 9). The wavelets are tested in 5th level and the shearlets in 3rd level of decomposition. Therefore, it is evident that the properties of the coarse coefficients of shearlets are noticeably better than those of wavelet sand they achieve a high identification rate.

Figure 10: Comparing of matching methods at *3rd* Shearlets Decomposition level.

Table 4: Results obtained from the proposed algorithm on utilized databases.

Database	Number of Images	Running Time (sec)	Accuracy (%)
DRIVE	500	0.92	EER = 0.0011
STARE	500	1.2	EER = 0.0018
Our Database	**5000**	**4.7**	**EER = 0.0024**

Experiments on distance methods

In order to obtain superior matching, we looked at the *Mahalanobis* distance (proposed matching distance) with other routine distance matching methods as defined: Euclidean, Hamming and *Mahalanobis* in 3rd shearlets transform decomposition level in furthermore; this figure demonstrates the outcomes (EER) of matching methods in different number of training pictures, what's more in different decomposition levels in our paper. Figure 10 clearly indicates that the identification performance of our proposed system (EER) for *Mahalanobis* distance enhances fundamentally at the point when more sample images are utilized as a part of the training stage as was supposed as this similarity distance, in examination with other matching methodologies. Along these lines, by expanding the training images we can gain more appropriate efficiency in proposed technique by utilizing *Mahalanobis* distance (Table 4).

Finally, some of state of the art identification approaches together with their results are presented in (Table 3). This enables researchers to conduct comparative studying with the existing works and assess their own work.

However, in order to test the performance of our algorithm, we used famous DRIVE and STARE database, in which they have 500 images after various rotate process, respectively, and the desired results were also achieved. It should be note that, in this paper the reason of using individual database in compare of existed databases is considering of various conditions in data capturing that mentioned in Section VII. Finally, (Table 4) shows a synopsis of the performance indicators based on all applied databases in the proposed algorithm.

Conclusion

In this paper, we presented an automated system for person identification based on the human retina. We used a three sections algorithm in this paper consisting of preprocessing, proposed methodology and feature matching. In the first step, in order to enhance performance of biometric identification system, we introduced rotation compensation method based on Radial Tchebichef Moments and further by localization of the optic disc, identified the retinal Region of Interest (ROI) to create the rotation invariant template from each retinal sample. The second steps involved introducing a multi-resolution analysis method based on shearlets transform. Following this, applying the proposed method, several features were extracted. In the third step, matching function that depends on *Mahalanobis* distance plays out a calculation to get an arrangement and earn an arrangement of similarity scores between the present biometric example and *N* saved biometric templates (1: N matching). In addition, we employed a special kind of distance to determine the similarity between the biometric patterns. Furthermore, it is possible to construct a multimodal identification by combining this technique with other biometric modalities in future works so that a new biometric identification system with greater efficiency can be achieved.

References

1. Jain K, Ross A, Prabhakar S. An Introduction to Biometric Recognition. IEEE Transactions on Circuits and Systems for Video Technology. 2004; 14.

2. Hoover A, Kouznetsova V, Goldbaum M. Locating Blood Vessels in Retinal Images by Piecewise Threshold Probing of a Matched Filter Response. IEEE Trans Med Imaging. 2000; 19.

3. Staal J, Abràmoff MD, Viergever MA, van Ginneken B. Ridge-Based Vessel Segmentation in Color Images of the Retina. IEEE Trans Med Imaging. 2004; 23.

4. Oinonen H, Forsvik H, Ruusuvuori P, Yli-Harja O, Voipio V, Huttunen H. Identity Verification Based on Vessel Matching from Fundus Images. 17th International Conference on Image Processing (Hong Kong). 2010.

5. J. Widjaja. Noise-robust low-contrast retinal recognition using compression-based joint wavelet transform correlator. Optics & Laser Technology Journal, Elsevier, Science Direct. 2015; 74: 97-102.

6. Waheed Z, Akram MU, Waheed A, Khan MA, Shaukat A, Ishaq M. Person identification using vascular and non-vascular retinal features. Computers and Electrical Engineering Journal, Elsevier, Science Direct. 2016; 53: 359-371.

7. Mukundan R, Ong SH, Lee PA. Image Analysis by Tchebichef Moments. IEEE Transactions on Image Processing. 2001; 10.

8. Hanaizumi H, Fujimura S. An automated method for registration of satellite remote sensing images. Proceedings of the International Geoscience and Remote Sensing Symposium IGARSS'93, Tokyo. 1993.

9. Lim WQ. The Discrete Shearlet Transform. A New Directional Transform and Compactly Supported Shearlet Frames. TIP. 2010.

10. Haralick RM, Shanmugam K, Dinstein I. Texural Features for image Classification. IEEE Transaction on System Man and Cybernetics. 1973; 3: 610-621.

11. Jain A, Nandakumar K, Ross A. Score Normalization in multimodal biometric systems. Pattern Recognition. 2005; 38: 2270-2285.

12. Kapoor S, Khanna S, Bhatia R. Facial gesture recognition using correlation and Mahalanobis distance. International Journal of Computer Science and Information Security (IJCSIS). 2010.

13. Chul-Hyun Park, Joon-Jae Lee, Mark J. T. Smith, Sang Park, Kil-Houm Park. Directional Filter Bank-Based Fingerprint Feature Extraction and Matching. IEEE Trans. Circuits and Systems for Video Technology. 2004; 14: 74-85.

14. Sukumaran S, Punithavalli M. Retina recognition based on fractal dimension. IJCSNS Int Journal. 2009.

15. Meng X, Yin Y, Yang G, Xi X. Retinal Identification Based on an Improved Circular Gabor Filter and Scale Invariant Feature Transform. Sensors (Basel). 2013; 13: 9248-9266.

16. Köse C, İki̇baş C. personal identification system using retinal vasculature in retinal fundus images. Expert System Journal. 2011; 38: 13670-13681.

17. Xu ZW, Guo XX, Hu XY, Cheng X. The blood vessel recognition of ocular fundus. Proceedings of the 4th International Conference on Machine Learning and Cybernetics Guangzhou. 2005.